

An immersed boundary framework for modelling the growth of individual cells: An application to the early tumour development

Katarzyna A. Rejniak*

Division of Mathematics, University of Dundee, Dundee DD1 4HN, Scotland, UK

Received 5 December 2006; received in revised form 22 February 2007; accepted 26 February 2007

Available online 12 March 2007

Abstract

A biomechanical approach in modelling the growth and division of a single fully deformable cell by using an immersed boundary method with distributed sources is presented, and its application to model the early tumour development is discussed. This mathematical technique couples a continuous description of a viscous incompressible cytoplasm with the dynamics of separate elastic cells, containing their own point nuclei, elastic plasma membranes with membrane receptors, and individually regulated cell processes. This model enables one to focus on the biomechanical properties of individual cells and on communication between cells and their microenvironment, simultaneously allowing for the formation of clusters or sheets of cells that act together as one complex tissue. Several examples of early tumours growing in various geometrical configurations and with distinct conditions of their initiation and progression are also presented to show the strength of our approach in modelling different topologies of the growing tissues in distinct biochemical conditions of the surrounding media.

© 2007 Elsevier Ltd. All rights reserved.

Keywords: Immersed boundary method; Growth of elastic cells; Formation of solid tumours

1. Introduction

A biomechanical approach in modelling the growth and division of a single deformable eukaryotic cell by using an immersed boundary method with distributed sources is presented here, and its application to model the early tumour development is discussed.

In the simplest view, a eukaryotic cell can be seen as built from a few distinct compartments: the nucleus containing the cell genetic material; the surrounding cytoplasm—a jelly-like substance consisting of liquid cytosol and various cellular organelles; the cell cytoskeleton composed of actins, microtubules and intermediate filaments playing an important role in defining the cell's organisation and shape; and the cell plasma membrane—a permeable lipid bilayer separating the intracellular elements from the external environment. All cell life processes depend on signals sensed locally by the cell from the cell microenviron-

ment that includes the surrounding extracellular matrix and other neighbouring cells. In principle, these signals may include concentrations of growth factors or nutrients dissolved in the surrounding media or mechanical attachments to other cells or to the extracellular matrix. The cell plasma membrane contains numerous proteins playing role of cell receptors and adhesion sites that enable separate cells to bind directly to one another and to send signals via chemical and electrical channels. Such communication mediated by specific membrane-surface receptors activates various intracellular signalling pathways and chemical reactions that take place in the liquid part of the cell cytoplasm made up of water, salts, organic molecules and enzymes that catalyse reactions. Several kinds of very specialised cell organelles play a crucial role in producing energy (mitochondria), protein synthesis (ribosomes, rough endoplasmic reticulum), lipid synthesis (smooth endoplasmic reticulum), protein sorting (Golgi apparatus), sequestering toxic materials (vacuoles) or digestion of macromolecules (lysosomes). A special part of the cell internal structure is the cortex—a dense network of actin

*Tel.: +44 1382 384476; fax: +44 1382 385516.

E-mail address: rejniak@maths.dundee.ac.uk.

filaments and proteins located near the cell plasma membrane, that gives the cell's surface its mechanical strength and enables its deformation and movement. A very detailed description of the cell structure can be found in classical textbooks (Alberts et al., 2002; Lodish et al., 2003; Pollard and Earnshaw, 2004). A schematic representation of the cell structure with those compartments that are important for our mathematical model is presented in Fig. 1.

Reproduction of the mammalian cell requires first an increase in the cell mass and doubling of its molecular contents, then DNA replication and separation take place and, finally, the entire cell splits physically into two daughter cells. An average size of the population of proliferating mammalian cells remains constant over time, even if cell divisions are nonsymmetric. The unevenly split daughter cells tend to return to the mean size after several divisions (Conlon et al., 2001; Conlon and Raff, 2003). Once the cell doubles its area, a complex multi-step process of cell mitosis takes place requiring replication of chromosomes (prophase), separation of sister chromatids (metaphase and anaphase), assembly of the contractile ring (telophase) and physical division of the mother cell (cytokinesis). Several mathematical models have been previously propounded to address different intracellular processes (for a review see Fall et al., 2002; Keener and Sneyd, 1998). Control of cell volume, regulated by the ionic pumps that maintain concentration differences across the cell membrane, and different properties of the cell plasma membrane have been addressed in Hoppensteadt and Peskin (1992), Keener and Sneyd (1998). Very detailed models of particular phases of the cell nuclear division have been offered in Cytrynbaum (2003a, b), Wollman et al. (2005). Cell deformability and break-up of capsules and viscous drops have been proposed as an idealization of the cell cytokinesis in Pozrikidis (2003), Cristini et al. (2001)

and Khismatullin et al. (2003). The mechanisms of the cleavage formation have been addressed in He and Dembo (1997). The cell metabolism and self-maintenance due to nutrients supplied by the environment have been modelled in Schwegler et al. (1985).

In the present work we introduce a computational technique based on an immersed boundary method in which the mechanical behaviour of the cell is captured as interactions between the cell elastic body and the viscous incompressible fluid representing the cell cytoplasm and the extracellular medium. Each cell is treated as an individual entity, with its own elastic plasma membrane, fluid cytoplasm, point nucleus and a set of discrete cell membrane receptors and adhesion molecules which enable connections between separate cells and allow cells to communicate with their surrounding microenvironment. Several biomechanical cell processes, such as individual cell growth, division and cell-to-cell communication are modelled within this framework. This computational technique will be applied to simulate the formation and development of solid tumours with various conditions of their initiation and progression. We will follow the general paradigm, that tumours arise from a single abnormal cell that has accumulated numerous genetic mutations over the life time of the host body (Alberts et al., 2002; Nowell, 1976). Such a cell gains certain proliferative properties and is able to escape from the growth controlling mechanism typical in normal cells, giving rise to a clone of similarly mutated cells. This proliferative advantage over the surrounding normal tissue results in further outgrowth of the mass of abnormal cells, called neoplasia. As long as these abnormal cells remain clustered together, the tumour is considered to be benign or solid. In contrast, if the cells are capable of breaking loose, invade the surrounding tissue, enter to the bloodstream and form secondary tumours by colonising the distant tissues (metastasis), the tumour is considered malignant. We will consider here only the initial phase of the tumour formation and development.

The present model of the growth of solid tumours differs significantly from previous continuum models (Bertuzzi and Gandolfi, 2000; Sherratt and Chaplain, 2001; Franks et al., 2005; Chaplain et al., 2006) and multiphase models (Lubkin and Jackson, 2002; Breward et al., 2002; Byrne et al., 2003; Byrne and Preziosi, 2003) that view tumours as cell densities; from hybrid discrete-continuous models (Anderson and Chaplain, 1998; Anderson et al., 2000; Anderson, 2005), cellular automata models (Patel et al., 2001; Dormann and Deutsch, 2002; Alarcón et al., 2003) and agent-based models (Mansury et al., 2002; Mansury and Deisboeck, 2003; Zhang et al., 2006) that view tumour cells as single points or single lattice sites; from cellular Potts models (Scott et al., 1999; Turner and Sherratt, 2002; Merks and Glazier, 2005) in which cells boundaries are defined on the fixed square grid; and from the centre-based models (Drasdo and Höhme, 2003, 2005; Galle et al., 2005) that trace cell nuclei only and assume a limited deformability of cell shapes. For a review of different

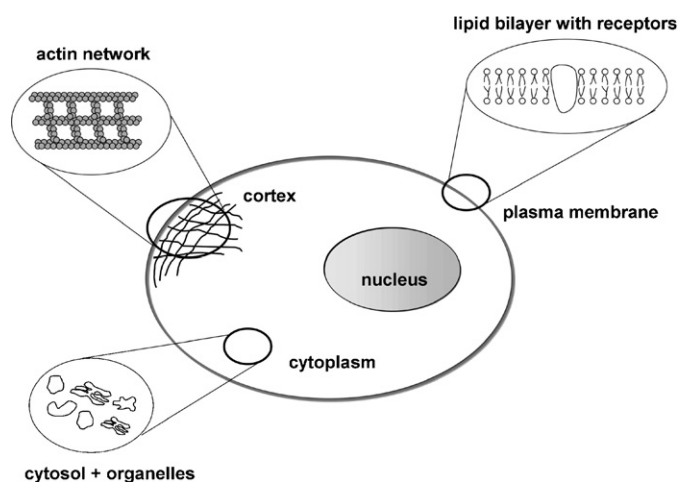


Fig. 1. A schematic structure of the eukaryotic cell. The cell nucleus is embedded in the cytoplasm consisting of fluid-like cytosol and various cell organelles and surrounded by the lipid plasma membrane that includes various cell receptors and is supported by a mesh of actins forming the cell cortex.

mathematical models of solid tumours and the related papers see Preziosi (2003), Friedman (2004), and Araujo and McElwain (2004). Our model allows for a more realistic representation of the tissue as a conglomerate of cells inhomogeneous in shape and behaviour. It contains a more detailed description of the mechanics of cell processes, that enables each cell to be a separate deformable entity with its own cell cycle and individually regulated and controlled cell processes. At the same time, however, all cells can communicate with their neighbours and can respond to microenvironmental signals, that results in a cooperative behaviour and acting as one complex tissue.

The remaining part of the paper is organised as follows. In Section 2, we outline the main features of the immersed boundary method, a mathematical framework used to model the behaviour of a single cell and whole tissue. In Section 3, we describe the structure of a eukaryotic cell and various cell processes, such as cell growth and division, cell adhesive properties and cell communication with its microenvironment. In Section 4, we present several computer simulations of growing clusters of tumour cells with distinct geometries and with different conditions of its growth initiation and progression. Several properties of our model are described in Section 5. Conclusions and some possible model extensions are discussed in Section 6. Numerical implementation of the complete system, an algorithm for solving it, and a set of physical and computational parameters used in simulations are all discussed in Appendix A.

2. Mathematical framework

The mathematical framework underlying our model is constituted by the immersed boundary method, that captures interactions between immersed elastic bodies and a surrounding incompressible viscous fluid. The fluid flow is influenced by sources of fluid distributed in the fluid domain, as well as by forces generated by the immersed elastic boundaries while, at the same time, the elastic structures move at the local fluid velocity. The immersed boundary method has been introduced by Peskin for the study of flow patterns around heart valves (Peskin, 1972) and then it was successfully applied to many problems in biological fluid dynamics. An exhaustive list of papers up to the year 2001 can be found in Section 9 of Peskin (2002). Recent papers include modelling of ciliary, flagellar and sperm motility (Dillon et al., 2003; Dillon and Fauci, 2006; Lim and Peskin, 2004), prosthetic mitral valves (Watton et al., 2007), simulations of the cochlea (Givelberg and Bunn, 2003), outgrowth of a chicken limb (Dillon and Othmer, 1999), development of tissue invaginations in the trophoblast bilayer (Rejniak et al., 2004), formation of tumour microregions (Rejniak, 2005) and development of different microarchitectures in intraductal tumours (Rejniak and Dillon, 2007).

In our model, the elastic bodies represent the tumour cells. The cell nucleus is modelled as a single point in which

the source of fluid is located if the host cell is growing. The boundary of each cell is modelled as a collection of massless springs applying a force to the fluid in which they are immersed. The cell membranes and cell nuclei are treated as neutrally buoyant bodies which are moved by the fluid at the local fluid velocity. Therefore, the mass is provided by the fluid, not by the cell membranes. We assume that the fluid inside the cells represents the cell cytoplasm and the fluid outside the cells represents the healthy, non-tumour tissue or the extracellular matrix. They both are modelled as the same homogeneous medium, but the lack of cell cytoskeleton and extracellular fibers is compensated for by choosing an adequately higher fluid viscosity (see Appendix A.3). Our choice to represent the cell cytoplasm and the extracellular matrix as simple homogeneous incompressible fluids is dictated by the fact that the immersed boundary method is grid dependent (see Appendix A.1) and the introduction of intracellular and extracellular elements requires a significant refinement of the fluid grid in order to capture computationally all additional details. We postulate that the motion of the fluid is governed by the Navier–Stokes equations (Batchelor, 2000; Peskin, 1977):

$$\rho \left(\frac{\partial \mathbf{u}}{\partial t} + (\mathbf{u} \cdot \nabla) \mathbf{u} \right) = -\nabla p + \mu \Delta \mathbf{u} + \frac{\mu}{3\rho} \nabla s + \mathbf{f},$$

$$\rho \nabla \cdot \mathbf{u} = s, \quad (1)$$

which describe the balance of momentum and the balance of mass in a viscous incompressible fluid with distributed sources. Here, ρ is the constant fluid density, μ is the constant fluid viscosity, \mathbf{u} is the fluid velocity, p is the fluid pressure, s is the fluid source distribution, and \mathbf{f} is the external force density. The fluid in our model is assumed to be incompressible, except at a discrete collection of isolated point sources which we use to model the growth of cells. Therefore the source distribution s and the local rate of fluid expansion $\nabla \cdot \mathbf{u}$ are identically equal to zero on the whole fluid domain except at these isolated points. Moreover, we require that the conservation of mass is preserved globally in the fluid domain Ω at each time t , that is, $\rho \int_{\Omega} (\nabla \cdot \mathbf{u}) \, \mathbf{d}\mathbf{x} = 0$.

The elastic cell boundaries are defined in the curvilinear coordinates $\mathbf{X}(l, t)$, where l is a position along the cell boundary. Note that l could be an arclength in the initial configuration. However, since cell membranes can undergo certain deformations, the distance between any two points along the boundary needs not to remain constant. The force density \mathbf{f} captures the forces $\mathbf{F}(l, t)$ defined at the elastic immersed boundaries of all cells $\mathbf{X}(l, t)$ in the following way:

$$\mathbf{f}(\mathbf{x}, t) = \int_{\Gamma} \mathbf{F}(l, t) \delta(\mathbf{x} - \mathbf{X}(l, t)) \, dl. \quad (2)$$

Here δ is the Dirac delta function, Γ is a finite collection of immersed boundaries of all cells and away from Γ , the external force \mathbf{f} is zero. The boundary forces $\mathbf{F}(l, t)$ include

the adjacent forces \mathbf{F}_{adj} , the cell-to-cell adhesion forces \mathbf{F}_{adh} and the contractile forces \mathbf{F}_{div} , which are all determined by the boundary configuration, the assumed elastic properties of the cell membranes and the undergoing cell processes. These forces are all described in Section 3.

The sources ($S_+ > 0$) of fluid are defined only at a finite collection of material points \mathcal{E}_+ representing nuclei of the growing cells with coordinates $\mathbf{Y}_k(t)$. The sinks ($S_- < 0$) are taken at a finite collection of points \mathcal{E}_- with coordinates $\mathbf{W}_m(t)$ located in the fluid domain in such a way as not to influence the behaviour of the whole tissue. Therefore, the source distribution is defined by:

$$s(\mathbf{x}, t) = \sum_{k \in \mathcal{E}_+} S_+(\mathbf{Y}_k, t) \delta(\mathbf{x} - \mathbf{Y}_k(t)) + \sum_{m \in \mathcal{E}_-} S_-(\mathbf{W}_m, t) \delta(\mathbf{x} - \mathbf{W}_m(t)). \quad (3)$$

In order to satisfy conservation of mass globally in the fluid domain Ω , we require that the total balance of source and sink distributions be equal to zero at every time t . Our choice of modelling the cell growth by using source–sink doublets is a simplification of the biological process in which the required fluid is recruited from the extracellular matrix by absorption through the cell membrane. However, such a simplified mechanism of fluid exchange describes adequately the overall dynamics of the growing cell and the developing tumour tissue. Moreover, the presented configuration of point sources and sinks is not critical for the computational results.

The material points of all immersed boundaries $\mathbf{X}(l, t)$ and the material points representing nuclei of the non-growing cells $\mathbf{Y}_k(t)$ move at the local fluid velocity. Thus, given a fluid velocity field $\mathbf{u}(\mathbf{x}, t)$, the local fluid velocity at the material points $\hat{\mathbf{X}}(t)$ (where $\hat{\mathbf{X}}(t)$ denotes either $\mathbf{X}(l, t)$ or $\mathbf{Y}_k(t)$) are determined using again the Dirac delta function. Integration is taken over the whole fluid domain Ω :

$$\frac{\partial \hat{\mathbf{X}}}{\partial t} = \mathbf{u}(\hat{\mathbf{X}}(t), t) = \int_{\Omega} \mathbf{u}(\mathbf{x}, t) \delta(\mathbf{x} - \hat{\mathbf{X}}(t)) d\mathbf{x}. \quad (4)$$

Numerical implementation of the complete system, an algorithm for solving it, and a set of physical and computational parameters used in simulations are all discussed in Appendix A.

3. Model of a eukaryotic cell

Our computational model of a eukaryotic cell includes several cell processes, such as cell growth and division, cell capability of sensing signals from its microenvironment, and cell adhesive properties. In this section we show how these processes are modelled within the immersed boundary framework. We start by describing cell structure (Section 3.1), cell microenvironment (Section 3.2) and cell adhesive abilities (Section 3.3). We end this section by presenting computational algorithms of the cell prolifera-

tion that includes cell growth, cell division and splitting into two daughter cells (Section 3.4).

3.1. Cell structure

The structure of the eukaryotic cell in our computational model includes several subcellular elements, such as the nucleus, the cytoplasm and the elastic plasma membrane, and several molecular complexes, such as the cell contractile ring, cell membrane receptors and cell adherens junctions. The elastic plasma membrane is modelled as a collection of points located on a simple closed curve. The elasticity of the plasma membrane derives from the fact that each boundary point is connected to its two adjacent neighbours by a linear spring satisfying Hooke's law with the constant resting length \mathcal{L}_{adj} and constant spring stiffness \mathcal{F}_{adj} . Thus the force $\mathbf{F}_{adj}(l, t)$ defined at a boundary point $\mathbf{X}(l, t)$ and exerted by an adjacent boundary point $\mathbf{X}(k, t)$ has the following form:

$$\mathbf{F}_{adj}(l, t) = \mathcal{F}_{adj} \frac{\|\mathbf{X}(k, t) - \mathbf{X}(l, t)\| - \mathcal{L}_{adj}}{\|\mathbf{X}(k, t) - \mathbf{X}(l, t)\|} (\mathbf{X}(k, t) - \mathbf{X}(l, t)). \quad (5)$$

The boundary points located on the cell membrane play an additional role of cell membrane receptors, that are used by the cell to communicate with its neighbours. Moreover, the same boundary points are treated as sites of potential cell-to-cell adhesion, that enables separate cells to form one compact tissue. Fig. 2 shows a portion of a small cluster of several eukaryotic cells with boundary points (dots), linear springs between adjacent points (thin lines) and adherent connections between neighbouring cells (thick lines).

3.2. Cell microenvironment

All cells can sense mechanical and chemical signals from their immediate neighbourhood and can also send mechanical signals to the neighbouring cells using adherent links or cell membrane receptors. However, this cell-to-cell

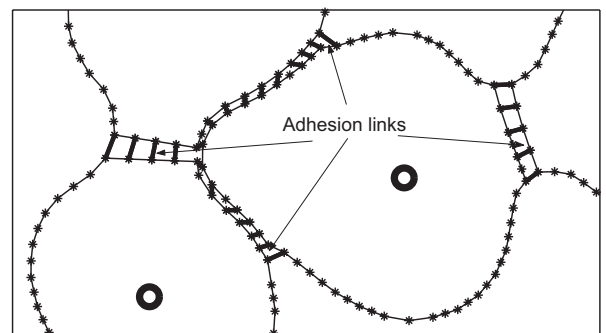


Fig. 2. A portion of a small cluster of several eukaryotic cells. The cell boundary points (dots) are connected by short linear springs (thin lines); cell nuclei (circles) are located inside the cell; separate cells are connected by the adherent links (thick lines). The cell cytoplasm enclosed by the plasma membrane is modelled as a viscous incompressible Newtonian fluid.

communication and information exchange can take place only within immediate neighbourhood of the cell, called the *cell microenvironment*. If \mathbf{X} denotes a point on the cell boundary, then its microenvironment $\Theta_{\mathbf{X}}$ is defined as a set of points lying within a distance ε , that is,

$$\Theta_{\mathbf{X}} = \{\mathbf{x}: \|\mathbf{x} - \mathbf{X}\| < \varepsilon\}. \quad (6)$$

The small parameter ε is called the *radius of the microenvironment*. Similarly, if $\Gamma = \{\mathbf{X}_k\}$ denotes the cell boundary (a collection of membrane receptors or membrane molecules), then the cell microenvironment Θ_{Γ} is defined as an ε -neighbourhood corresponding to the local area around the cell plasma membrane, that is,

$$\Theta_{\Gamma} = \bigcup_{\mathbf{X}_k \in \Gamma} \{\mathbf{x}: \|\mathbf{x} - \mathbf{X}_k\| < \varepsilon\}. \quad (7)$$

3.3. Cell-to-cell adhesion

Separate cells form a tissue by adhering to their neighbours using transmembrane adhesion proteins. We model such connections by introducing linear springs attached at the boundary points of two distinct cells if they are within their adhesion microenvironment of radius \mathcal{L}_{adh}^{max} . Thus, the adhesive force $\mathbf{F}_{adh}(l, t)$ defined at the boundary point $\mathbf{X}(l, t)$ and exerted by the boundary point $\mathbf{X}(k, t)$ belonging to a distinct cell has the following form:

$$\mathbf{F}_{adh}(l, t) = \mathcal{F}_{adh} \frac{\|\mathbf{X}(k, t) - \mathbf{X}(l, t)\| - \mathcal{L}_{adh}}{\|\mathbf{X}(k, t) - \mathbf{X}(l, t)\|} (\mathbf{X}(k, t) - \mathbf{X}(l, t)), \quad (8)$$

provided $\|\mathbf{X}(k, t) - \mathbf{X}(l, t)\| \leq \mathcal{L}_{adh}^{max}$ and is zero otherwise. Here, \mathcal{L}_{adh} is a constant resting length and \mathcal{F}_{adh} is a constant spring stiffness. Note that if both boundary points are within a distance smaller than the resting length \mathcal{L}_{adh} , then the acting force \mathbf{F}_{adh} is repulsive.

The process of cell-to-cell attachment and detachment in real cells is very dynamic (compare experimental movies in Alberts et al., 2002) and depends on the distance between neighbouring cells and on the kind of receptors expressed on cell membranes. In our model, all membrane receptors are considered identical, so the rearrangement of adhesive connections depends only on the distance between separate cells. Each cell can sense the presence of other cells in its adhesion microenvironment of radius \mathcal{L}_{adh}^{max} and can respond accordingly. New connections

are formed if the boundary points of two separate cells move within the prescribed adhesion distance \mathcal{L}_{adh}^{max} , but the existing adhesion links are disconnected if the corresponding boundary points move apart at a distance larger than \mathcal{L}_{adh}^{max} .

3.4. Cell proliferation

Cell proliferation is modelled by including all its mechanical phases, such as cell growth and shape elongation, formation of the contractile ring, the contractile furrow, and separation of daughter cells into two new entities with their own nuclei surrounded by the cytoplasm and enclosed by the plasma membrane. A few snapshots from a computer simulation of cell proliferation are presented in Fig. 3. We start the process of cell growth by introducing a point source inside the cell (Fig. 3a) that creates a fluid flow causing the cell to grow by pushing its boundaries and by increasing its area. This source is inactivated when the cell area doubles the size of its mother cell. At this time, two new nuclei are placed along the cell's longest axis and a contractile ring is created by introducing contractile forces that act on the opposite sides of the cell boundary (Fig. 3b). This results in a formation of a contractile furrow (Fig. 3c) and causes the division of the cell into two daughter cells of approximately equal areas and with their own nuclei (Fig. 3d). As the cell area increases during the growth cycle, additional immersed boundary points are added to model the growth of the cell membrane.

The strength of each point source S_+ located at the point $\mathbf{Y}_k(t)$ has the form of a step function, and is equal to a positive constant \mathcal{S}_0 over the time of cell growth, that is, from the time of growth initiation t_{init} to the time when the cell area is doubled t_{double} . After that, the fluid sources are inactivated. Therefore, the strength of each source is defined as follows:

$$S_+(\mathbf{Y}_k(t), t) = \begin{cases} 0 & \text{if } t < t_{init}, \\ \mathcal{S}_0 & \text{if } t_{init} \leq t \leq t_{double}, \\ 0 & \text{if } t_{double} < t. \end{cases} \quad (9)$$

The value of \mathcal{S}_0 needs to be determined computationally or experimentally, to match the dynamics of the growing living cell.

To conserve the overall mass of fluid in the considered domain, we introduce artificially a collection of small

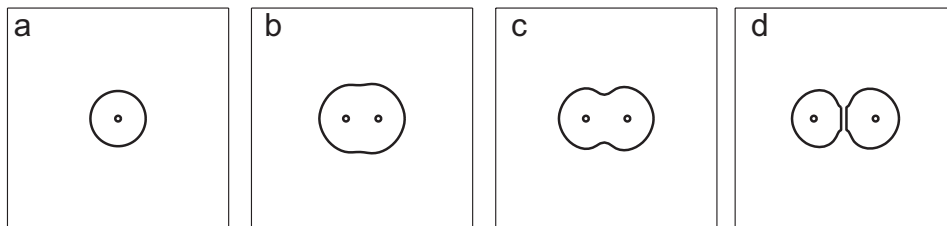


Fig. 3. Main mechanical phases of cell proliferation: (a) a cell ready to grow, (b) doubling the area and formation of the contractile ring, (c) cellular division, and (d) formation of two daughter cells.

balancing point sinks, located in the fluid domain in such a way so to not influence the behaviour of other cells and the whole tissue. The strength of fluid sinks S_- located at points $\mathbf{W}_m(t)$ is chosen in a way to balance the strengths of fluid sources located in growing cells. Thus, if K cells are growing, then the strength of each of M fluid sinks is equal to:

$$S_-(\mathbf{W}_m(t), t) = \frac{1}{M} \sum_{k=1}^K S_+(\mathbf{Y}_k(t), t). \quad (10)$$

In some specialised tissues, like the epithelial sheets or the cytotrophoblast layers, cells are highly polarised and thus the location of the spindle poles and the direction of cell growth are quite strictly determined. Every improper cell division in such tissues results in cell death or its differentiation. However, many tumour cells lose their polarised properties and their orientation seems to be independent of the orientation of their neighbouring cells. In our model, the shape and orientation of the growing cell depend on an actual configuration of cell boundary points. We assume that if the growing cell is not circular when its area is doubled, then the contractile ring is located orthogonally to the longest axis of the cell (a line passing through two the most distant points on the cell boundary) in such a way that the areas of both cell parts are approximately equal. If the cell is circular, then the contractile ring is located along a randomly chosen axis of the cell. The contractile forces cause the formation of a contractile furrow which separates the cell into two compartments. When the opposite boundary points are close enough, say within a distance \mathcal{L}_{div}^{min} , the contractile forces are inactivated and both cell compartments are split into two separate daughter cells. The algorithms of cell growth and division are illustrated in Fig. 4 for an indicated non-circular cell.

The contractile force $\mathbf{F}_{div}(l, t)$ defined at the boundary point $\mathbf{X}(l, t)$ and exerted by an opposite boundary point $\mathbf{X}(k, t)$ with a constant spring stiffness \mathcal{F}_{div} and the separation distance \mathcal{L}_{div}^{min} has the following form:

$$\mathbf{F}_{div}(l, t) = \begin{cases} \mathcal{F}_{div}(\mathbf{X}(k, t) - \mathbf{X}(l, t)) & \text{if } \|\mathbf{X}(k, t) - \mathbf{X}(l, t)\| \geq \mathcal{L}_{div}^{min}, \\ 0 & \text{otherwise.} \end{cases} \quad (11)$$

The value of the spring stiffness constant \mathcal{F}_{div} needs to be determined computationally or experimentally in a way to resemble the dynamics of cytokinesis in the living cell.

4. Computational results

To show a range of possible applications of our model of growing elastic cells we present four simulations of the development of solid tumours under different conditions of their initiation and progression. Two simulations (Sections 4.1 and 4.2) show the formation of multicellular tumour clusters where growing cells are chosen either randomly or depending on the concentration of external factors. Both simulations are considered to be test cases for the method and will be compared to experimental data and to results from other models. Two other simulations (Section 4.3) show growth of intraductal tumours and different tumour patterns, and will be used to discuss these features of our method that distinguish it from other single-cell-based models. We assume that during the time of tumour development referred to in our simulations, every cell is a subject to the same behavioural laws, despite its age and generation. In particular, we assume no occurrences of genetic mutations which could influence the cell cycle. Therefore, the following scenario is employed in all our simulations. An indicated cell will undergo the process of cell proliferation which results in the formation of two daughter cells connected by adhesion links. These cells will then grow and divide, forming new pairs of daughter cells which adhere to their closest neighbours forming one tumour cluster. This cluster will continue to develop from the growth of individual cells. Simulations presented in the next three sections differ in conditions of the initiation of cell growth (random vs. nutrient or environment dependent) and in the resulting tumour structure (unstructured solid vs. multilayered or patterned).

4.1. Modelling randomly growing clusters of tumour cells

We first use our model to show how the consecutive applications of our general algorithm for the growth and division of a single cell can produce a large cluster of cells forming one compact tumour tissue. In this case we start with a single mutant cell that upon uncontrolled divisions

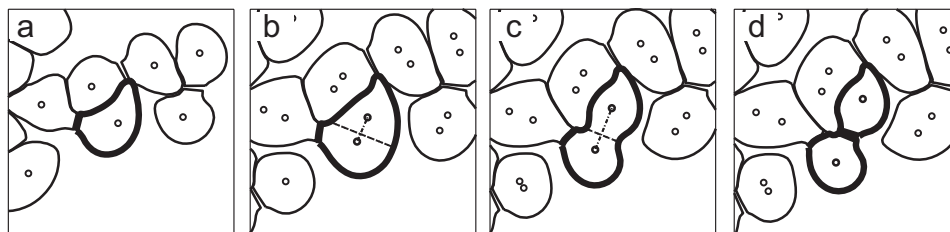


Fig. 4. Growth and division of one non-circular cell indicated by a thick line: (a) an irregularly shaped cell ready to proliferate, (b) location of the contractile ring (dashed line), (c) cell division along the contractile connection, and (d) formation of two daughter cells.

gives rise to a clonal tumour expansion. This situation corresponds to the early development of multicellular spheroids growing in the environment rich in nutrients. Such experimental systems are the *in vitro* models of avascular tumours. We follow the formation of a cluster of tumour cells starting from one cell of $10\ \mu\text{m}$ in diameter and finally reaching about 700 cells in its two-dimensional cross section. Since we model here very small tumours growing in the environment rich in nutrients, every cell in our system is able to grow independently of its location within the cluster. Therefore, we initiate a process of proliferation in a cell selected randomly from among all cells that are ready to proliferate. This takes place in time intervals corresponding to about 10 min of simulated time to match experimental observations that only a small fraction (below 10%) of all tumour cells within a multicellular spheroid are actively dividing at any given time (Sutherland et al., 1971). Once a cell is chosen to

proliferate, it grows and divides independently of its neighbours. Moreover, the fact whether the cell enters into a particular phase of cell proliferation depends entirely on the state of this cell and on the configuration of cell boundary points.

Several snapshots showing formation of a multicellular spheroid over the time period of about six days are shown in Figs. 5a–i. The first six images are taken at time intervals of 8.5 h and show an early phase of tumour growth and its self-organisation into a compact cluster, whereas the final three images are taken at time intervals of 42.5 h and show further tumour expansion. We start this simulation with a single circular cell, Fig. 5a, that undergoes a process of cell growth and division resulting in the formation of two daughter cells, Fig. 5b. Uncontrolled divisions of these cells give rise to small cell aggregates of irregular elongated shapes, Figs. 5c–d. This is due to the fact that some of the growing cells have only one neighbour around to form

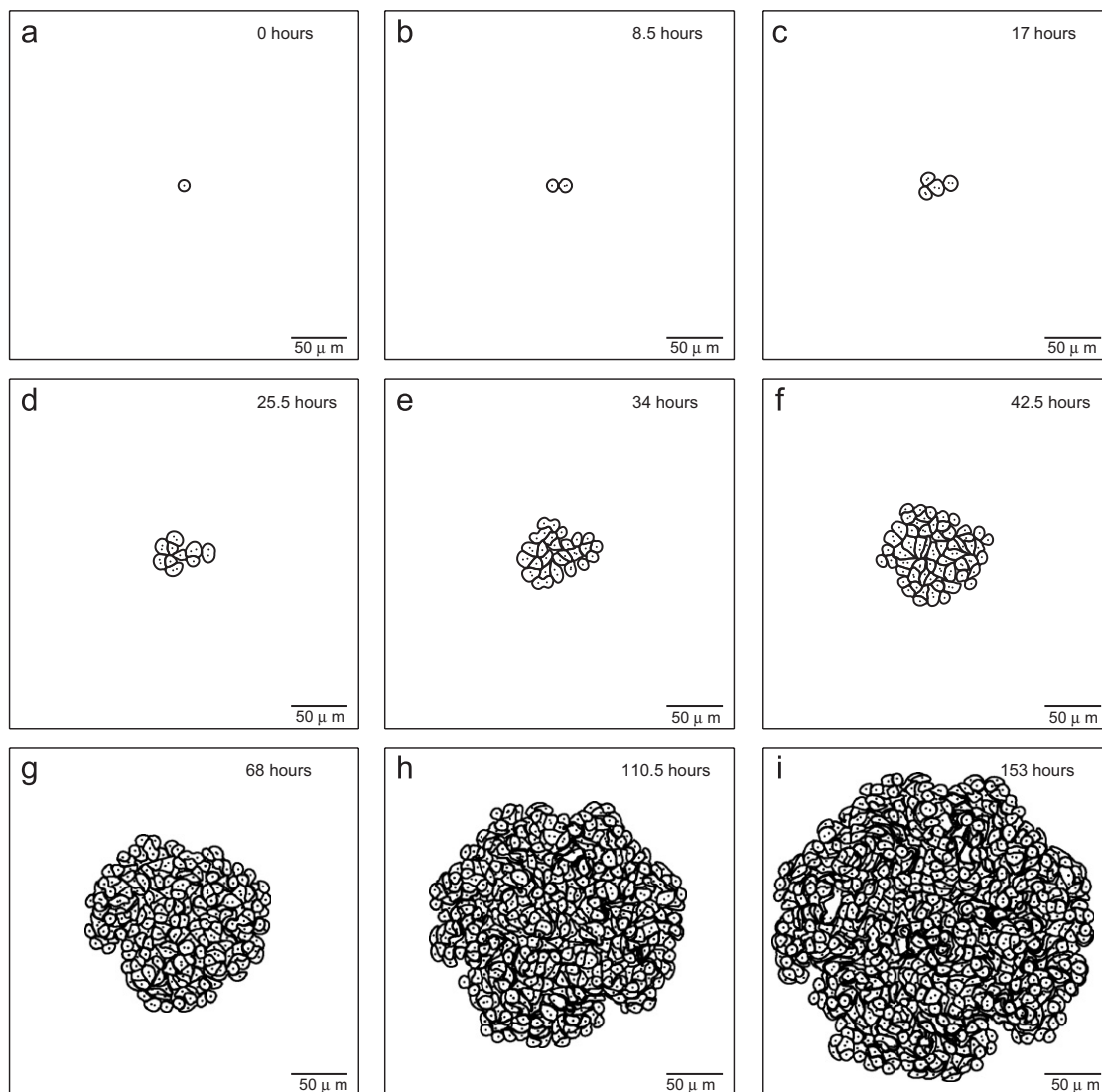


Fig. 5. Development of the cross section of a solid tumour: (a) one cell of diameter $10\ \mu\text{m}$, (b) two cell aggregate, (c) four cell aggregate, area of $0.00048\ \text{mm}^2$, (d) 10 cells, area $0.0011\ \text{mm}^2$, (e) cluster of 25 cells, area $0.0026\ \text{mm}^2$, (f) 59 cells, area $0.0055\ \text{mm}^2$, diameter $0.099\ \text{mm}$. (g) 205 cells, area $0.018\ \text{mm}^2$, diameter $0.16\ \text{mm}$; (h) 453 cells, area $0.041\ \text{mm}^2$, diameter $0.22\ \text{mm}$; (i) 703 cells, area $0.077\ \text{mm}^2$, diameter $0.28\ \text{mm}$; Bars equal to $50\ \mu\text{m}$.

adhesive connections with, however, all of them have still circular or elliptical shapes. When the number of cells increases, more cell-to-cell adhesion links are formed and the tumour shape becomes more compact and roundish, Figs. 5e–f. Here, the shape of a particular cell depends on its location within the cluster. The centrally located cells become more polygonal in shape as they develop adhesion connections to cells located around them, whereas the cells located at the outside surface of the cluster are still more circular. Larger clusters form conglomerates of cells inhomogeneous in shape with no common orientation and in different phases of the cell proliferation process, Figs. 5g–i. Only cells located on the tumour surface can grow freely, whereas cells located inside the tumour cluster are exposed to increased pressure from the surrounding cells. This results in higher accumulation of cell bodies inside the tumour cluster.

Our simulation is consistent with the experimental data on early development of multicellular spheroids presented in Sutherland et al. (1971). In both cases the exponential growth takes place over the period of four days with a significant reduction of growth rate after that time. It is also reported in Sutherland et al. (1971) that the mitotic events are uniformly distributed in spheroids smaller than 150 μm in diameter, and in larger clusters the proliferating cells are not present in the central part of the cluster; however, those cells are still mitotically viable. The same can be observed in our model, where initially the growing cells are visible in the whole cluster, but once the cells in the centre are too crowded to freely grow, the mitotic events are confined to the most external zone of the cluster.

4.2. Nutrient-dependent tumour growth

Our basic model of a growing cluster of tumour cells has been extended in Rejniak (2005) to include some external factors, such as concentrations of oxygen, nutrients or growth factors, that regulate the life processes of each individual cell in the cluster. To reduce the computational complexity, the kinetics of all chemical gradients is defined in this model on the already existing regular fluid grid and their uptake (or degradation) by the tumour cells in the already identified local cell microenvironments. In the example considered here we use only one external factor γ and assume that the cell growth is dependent on its concentration sensed by the cell. Therefore the fluid source function S_+ defined in Eq. (3) to model cell growth depends here on the concentration of γ at the material points of cell nuclei $\mathbf{Y}_k(t)$:

$$S_+ = S_+(\gamma(\mathbf{Y}_k, t), t), \tag{12}$$

and the value of γ at the material point \mathbf{Y}_k is equal to its local concentration around that point:

$$\gamma(\mathbf{Y}_k, t) = \int_{\Omega} \gamma(\mathbf{x}, t) \delta(\mathbf{x} - \mathbf{Y}_k(t)) \, d\mathbf{x}. \tag{13}$$

We assume that the dynamics of the factor γ comes only from its uniform diffusion in the whole computational domain (with the diffusion coefficient \mathcal{D}_γ) and its degradation, defined using the Michealis–Menten formulation (with a maximal consumption rate \mathcal{V}_γ and the Michaelis constant κ_γ) that takes place only near boundaries Γ of tumour cells, that is, within the cell microenvironment Θ_Γ . Initially the whole computational domain Ω is filled uniformly with an optimal concentration γ_0 of the considered factor. Moreover, a constant source of value γ_0 is continuously applied at the domain boundaries. The rate of change of γ in the whole domain is defined by the reaction-diffusion equation with the following boundary and initial conditions:

$$\frac{\partial \gamma(\mathbf{x}, t)}{\partial t} = \mathcal{D}_\gamma \Delta \gamma(\mathbf{x}, t) - \mathcal{V}_\gamma \frac{\gamma(\mathbf{x}, t)}{\kappa_\gamma + \gamma(\mathbf{x}, t)} \cdot \chi_{\Theta_\Gamma}(\mathbf{x}), \tag{14}$$

$$\begin{aligned} \gamma(\mathbf{x}, t_0) &= \gamma_0 \quad \text{for } \mathbf{x} \in \Omega, \\ \gamma(\mathbf{x}, t) &= \gamma_0 \quad \text{for } \mathbf{x} \in \partial\Omega \quad \text{and } t \geq t_0, \end{aligned}$$

here, χ is a set characteristic function defined as:

$$\chi_{\mathcal{A}}(\mathbf{x}) = \begin{cases} 1 & \mathbf{x} \in \mathcal{A} \\ 0 & \mathbf{x} \notin \mathcal{A} \end{cases}.$$

As in the previous case, the process of cell proliferation is initiated in one cell at a time, but here the cell selection is based on the highest concentration of γ sensed by all cells from their microenvironments. The factor γ in turn is degraded in the areas close to the cell boundaries, and if its concentration falls below the γ_{min} level in the vicinity of a particular cell, that cell becomes necrotic and cannot be further selected to grow. Therefore, the fate of each cell depends entirely on the evolution of γ in the cell microenvironment, and the evolution of γ depends on the location of boundaries of all tumour cells. As a result of this coupling, there is a competition between the cells for the factor γ that leads to the formation of three phenotypically different tumour subpopulations. The proliferating cells sense high concentrations of γ and are actively growing and dividing. The quiescent cells sense low concentrations of γ and are resting, but they can re-enter the proliferating phase if the concentration of γ increases in their microenvironments. The necrotic cells are dying due to the lack of γ in their microenvironments and are not able to re-enter the proliferating phase. In consequence, three distinct tumour microregions are formed that differ in concentration of γ and are occupied by cells of different phenotypes.

Fig. 6 shows the results of one computational simulation initiated from a cluster of seven cells placed in the centre of the domain that has been filled with a uniform concentration of the external factor γ (data not shown). Initially, all cells sense high concentrations of γ around them, and subsequently start proliferating which leads to the formation of an aggregate of growing cells, Fig. 6a (growing cells are coloured in grey). Degradation of γ by tumour cells

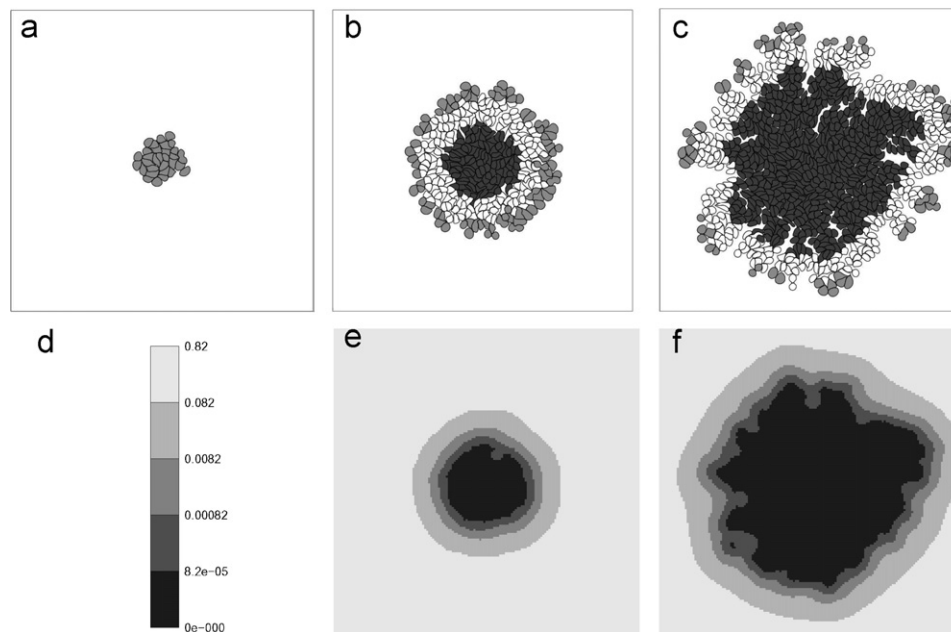


Fig. 6. Development of nutrient-driven tumours: (a)–(c) spatial distribution of subpopulations of tumour cells: necrotic—black, proliferating—grey; viable—white; (e)–(f) spatial distribution of γ corresponding to cases (b)–(c); the concentration variability in case (a) is not shown since it is insignificantly small; (d) a colour bar for the gradient of γ [mM].

leads to the formation of its gradient (Fig. 6e) that in turn causes cell's starvation and their necrotic death in the areas of γ depletion. Fig. 6b shows three subpopulations of tumour cells: centrally located necrotic core (black cells), a rim of proliferating cells outside the cluster (grey cells), and a ring of quiescent cells in between (white cells). At this stage, the tumour still has a roundish shape which shows that the cell competition for the factor γ is not yet very strong, and most outer cells sense γ in a concentration sufficient for their growth. However, a closer inspection of the tumour boundaries reveals its irregularities that will lead to the formation of finger-like structures growing towards the areas of higher concentrations of γ , Fig. 6c. The quiescent cells sense such concentrations of γ that allow them to maintain some cell life processes and to avoid death by starvation, but they are not high enough to enable initiation of their growth, Fig. 6f. The spatial distribution of the concentration of γ corresponding to the tumour cluster in Fig. 6a is not shown, since the concentration variability in this case is insignificantly small.

The presented results showing the development of a three-layered tumour structure are in qualitative agreement with classical experimental data on the growth of multicellular spheroids (Folkman and Hochberg, 1973; Sutherland, 1988; Mueller-Klieser, 1978). Our simulation also produces similar profiles of oxygen consumption characterised by a near-zero plateau around the central necrotic core, and a steep gradient of oxygen concentration increasing towards the outer rim of proliferating cells. Moreover, the tumour structure produced by our model is comparable with results obtained from other single-cell-based models (such as, cellular automata models

Anderson, 2005; Dormann and Deutsch, 2002; Kansal et al., 2000, cell-centred models, Drasdo and Höhme, 2005 or cellular Potts models, Scott et al., 1999; Jiang et al., 2005), even if the underlying mechanisms of cell growth and nutrients consumption are significantly different. For instance, all cells in our model have fully deformable shapes, whereas in cellular automata models cells are defined as single sides on the lattice, and in off-lattice cell-centred models cells are modelled as overlapping spheres of limited deformability. The processes of cell growth and division are time dependent in our model, that is in contrast to cellular automata models where cell reproduction is achieved during one iteration step only. In cell-centred and cellular Potts models the process of cell proliferation is indeed time dependent, but our model is able to capture more realistic continuous transformations of the morphology of growing and dividing cells. In our model nutrients consumption takes place along the cell membranes that allows cells to sense different concentrations of external factors from different directions. In contrast, in cellular automata and cell-centred models all cells sense only an average nutrients concentration, since the same lattice is used for cell and nutrients allocation in the former case, and the nutrient uptake takes place only around the cell centres in the latter case. Despite these eminent differences in the mechanisms of cell growth and nutrients uptake, the final results of two presented test cases—the formation of one compact cluster from randomly selected growing cells (Section 4.1) and the emergence of a three-layered tumour cluster in nutrient-dependent cell growth (this section)—are comparable with simulations from other single-cell-based models.

4.3. Development of intraductal tumours

We now show that our framework for the multicellular growth is not limited to the case of cell clusters growing freely in the homogeneous media, but in fact it is relatively easy to include in our model different cell environments and distinct geometries of growing tissues. We show two examples of tumours growing inside either the linear or circular cross sections of epithelial ducts. We also show how incorporation of different conditions of cell growth may result in either a random or patterned development of such tumours. The initial configurations in both cases discussed below consist of the hollow lumen (of a linear or circular shape) enclosed within a layer of epithelial cells and surrounded by a stiff basement membrane that supports the tumour growth inside the lumen. This configuration corresponds to the geometry of a normal epithelial duct. Tumoural growth is initiated in some epithelial cells along the duct and the final pattern is achieved by consecutive proliferations of daughter cells.

Figs. 7a–d show the tumour growing inside a circular cross section of the epithelial duct in the form of long fronds protruding into the lumen. This tumour has been initiated in four particularly chosen epithelial cells along the duct and finally develops into four slender finger-like structures intersecting randomly inside the duct. This tumour architecture, known as a micropapillary pattern, is a result of specific rules of cell proliferations that reduce tumour outgrowth only to the cells located on the tips of the protrusions. In contrast, Figs. 7e–h show the tumour growing inside a linear cross section of the epithelial duct in the form of an unstructured mass of cells that are randomly oriented. The growth of this tumour has been also initiated

in four particularly chosen cells along the duct, but when a small cluster of tumour cells is formed, all further proliferations are initiated in randomly selected daughter cells. This cell pattern resembles the form of solid tumours. In both cases the basement membrane is intact and the integrity of epithelial layers is maintained, however, some of the epithelial cells near the growing tumours are deformed.

Several different patterns of intraductal tumours, that have been simulated by our model, are discussed in more detail and compared to real pathology samples in Rejniak and Dillon (2007). This particular application shows also some features of our model that are not easily achieved in other single-cell-based models, that clearly distinguishes our approach from other techniques. Since all cells in our model are fully deformable, this allows for a real representation of the whole tissue as a conglomerate of cells inhomogeneous in their shapes due to cell competition for space during their growth (solid tumour), but also enables a structured assemble of cells in the form of long fronds protruding into the lumen (micropapillary tumour) or an epithelium layer (either linear in the solid tumour case, or circular in the case of micropapillary carcinoma). Moreover, since all cell-to-cell interactions are defined on a level of cell receptors, the adherent–repulsive forces acting between growing cells lead to a natural cell polarity in the micropapillary tumour, but to a randomly oriented cells in the solid tumour. The micropapillary pattern is formed by slowly growing top cells that form relatively rare connections with their neighbours, so their shapes remain ellipsoidal with orientation toward the centre of the duct that results in similar locations of the division axis among all dividing cells. In contrast, in solid tumour all cells grow

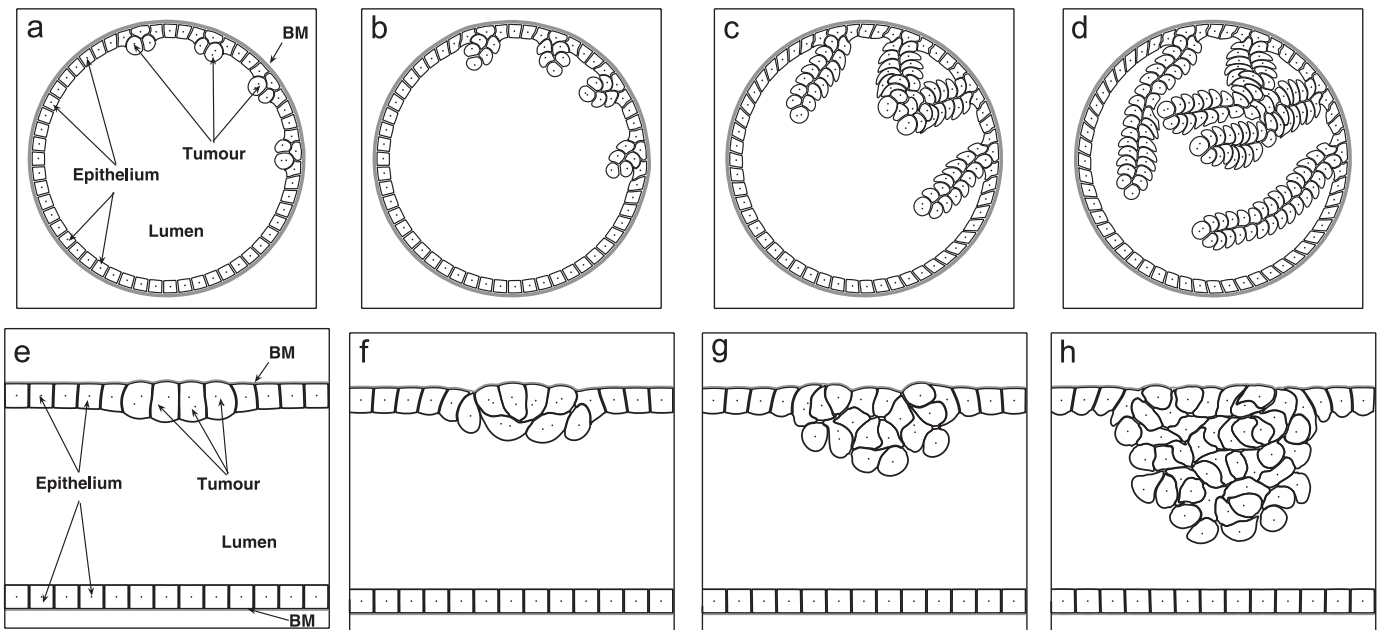


Fig. 7. Growth of intraductal tumours shown in the circular (a)–(d) and linear (e)–(h) cross sections through the hollow duct composed of one layer of epithelial cells (squares) and surrounded by the stiff basement membrane (thick grey lines); tumour growth is initiated in some epithelial cells and progresses by partially filling the duct. Figs. (a) and (e) show locations of the epithelial and tumoural cells, the lumen, and the basement membranes (BM).

fast forming multiple connections with their neighbours that results in their polygonal shapes and subsequently in differently oriented axis of cell division, that results in the final configuration showing random orientation of all tumour cells. Such directly defined cell-to-cell adhesion allows individual cells to feel presence of other cells in their neighbourhoods, and may prevent cells from growing if they are too crowded to do so, such as cells located inside the solid tumour cluster.

In this model we introduced a few biological structures, that did not appear in the previous models, such as the basement membranes and layers of epithelial cells. They all can be incorporated into our model as additional immersed bodies and their elastic or stiff properties can be achieved by adequately chosen values of spring stiffness. Adding these new structures to the whole system is computationally inexpensive, since the immersed boundary method makes use of the fixed fluid grid, and no fluid grid rearrangement is needed when new immersed bodies are introduced. In particular, each epithelial cell in the simulations discussed here is defined exactly as described in Section 3, however, here the cells acquire rectangular shapes and are arranged in one circular or two linear layers. The basement membrane is modelled as an additional stiff body and is represented by a discrete collection of Lagrangian points $\{\mathbf{Z}_l(t)\}$ forming two interconnected curves. Each boundary point is connected to its two neighbours on the same curve and to its two neighbours on the other curve by the adjacent linear springs \mathbf{F}_{adj} defined similarly to the adjacent springs acting in the cell boundaries, Eq. (5). Moreover, the most inner curve of the basement membrane is connected to the neighbouring epithelial cells by adherent springs \mathbf{F}_{adh} defined similarly to adherent springs acting between epithelial cells, Eq. (8). Additionally, to keep the basement membrane intact, each boundary point $\mathbf{Z}_l(t)$ is connected to its initial location $\mathbf{Z}_l^i(t)$ by a linear tethered spring \mathbf{F}_{th} with a constant spring stiffness \mathcal{F}_{th} :

$$\mathbf{F}_{th}(l, t) = \mathcal{F}_{th}(\mathbf{Z}_l(t) - \mathbf{Z}_l^i(t)). \quad (15)$$

All boundary points of the epithelial cells and the basement membranes are moved at the local fluid velocity as given in Eq. (4), in exactly the same way as all other material points. However, since the basement membrane is supposed to be immobile, the tethered forces need to be very stiff comparing to other forces acting on the basement membranes.

4.4. Conclusions on defining the details of the model

The presented here model of a growing elastic cell that uses the immersed boundary framework is quite general and gives some freedom in defining certain elements of the model. A general principle followed in our approach is that the cells are modelled as elastic bodies immersed in the viscous incompressible fluid and its motion is influenced by various forces acting on the boundaries of all cells and by

sources and sinks of fluid used to model cell growth. Particular versions of this general method may differ in the design of the structure of cell membranes, in the location of sources and sinks of the fluid around the growing cells, and in defining algorithms for selection of the mitotic orientation during the cell division. In the model presented here, the cell membrane is represented by one closed curve and each boundary point on this curve is connected to its two neighbours (one on each side) by short linear springs. That could be altered by introducing a more complex structure. For instance, the cell membrane may consist of two closed curves that are interconnected by a mesh of short linear springs, that will provide more resistance to its deformation, but will also increase the computational cost of the model. In a current version the cell cytoplasm is modelled as a homogeneous fluid, but it is possible to include more detailed representation of some cell organelles and the cell cytoskeleton, for instance, as an additional network of elastic springs that can be used to model bundles of actin filaments or microtubular structures; this approach in modelling the cell cytoskeleton within a framework of the immersed boundary method has already been used by Bottino to model a crawling amoeba (Bottino and Fauci, 1998; Bottino, 1998). Similarly, a more realistic model of the extracellular matrix may include some stromal cells, such as fibroblasts, or macrophages, or the fibres of collagen, or laminin, modelled as additional springs and spring networks embedded in the fluid. This, again, will increase the computational cost of the model. In all simulations presented here, the cell growth is modelled by placing a single source of fluid in the cell nucleus and several balancing sinks outside the cell boundaries. A more biologically relevant way to model the transport of fluid through the boundary of a growing cell would be to place pairs of fluid sources and sinks along the cell boundary in the form of discrete channels. The orientation of cell division in all simulations presented here is chosen to be orthogonal to the cell's longest axis, but different rules can be introduced for determining the location of the contractile ring. This short list of possible modifications of our model of growing elastic cells shows that the modeller has a certain degree of freedom in defining some model details and allows the modeler to find balance between the true representation of biological structures and the computational costs needed for simulations.

5. Properties of the model

Since all biomechanical processes have been defined in our model on the level of single cells or small cell aggregates, and then employed in simulations involving hundreds of interacting cells, it is important to analyse the behaviour of individual cells in such large communities, especially that single cells are under pressure from their neighbours. We expect from the model that the cell properties stay roughly the same even if the number of cells in the cluster is large. The following aspects of cell life

are subject of our tests: time needed for the growth and division of individual cells, Section 5.1; preservation of the areas of daughter cells directly after the division of their mother cell, Section 5.2; preservation of the area of the non-growing cells, Section 5.3. We also inspect how each growing cell contributes to the growth of the whole tumour cluster by analysing simultaneously an increase in the total number of tumour cells and an enlargement of the total tumour area, Section 5.4. The analysis will be performed on the data collected from the simulation of randomly growing clusters of tumour cells, Section 4.1.

5.1. Time of cell growth and division

We assume that the process of cell growth is completed when the cell area is doubled. Similarly, the process of cell division is finished when the opposite sides of the contractile furrow approach each other within the distance of the mesh width. During the simulation we monitor the areas of all growing cells and the depth of the contractile furrows in all dividing cells, but we do not restrain the time needed to complete these processes. Therefore, this time can be different for different cells. The time distribution of the doubling of cell areas and of the ingress of the contractile furrow for 90 cells from a simulation of the randomly growing cluster of tumour cells (Section 4.1) are shown in Figs. 8a and b, respectively. The average time

needed to double cell area is about five and half hours. In most of the 90 cases considered here, this doubling time falls within the 10% interval from the mean. The few exceptions are due to uneven cell division and in these cases the daughter cells need respectively more or less time to reach the desired doubling of the area of their mother cells. This is important in keeping a uniform size of cell population; otherwise the cell area of each next generation would be diminished. Moreover, the exemptions from the average doubling time occur more often in large clusters. This follows from the fact that more cells are located inside the cluster and surrounded by other cells that give resistance to the growing cell and cause an increase in the cell doubling time. The time needed to complete the process of cell division is quite uniform, and for almost all considered cells, falls within the 10% interval from the average of 29.24 min. This is consistent with experimental data on mitosis and cytokinesis in epithelial cells (Alberts et al., 2002, pp. 1034–1035).

5.2. Division of the mother cell

The proliferating mother cell must first double its size before it splits into two daughter cells of approximately equal areas. We generally expect that the areas of all cells in the cluster should be roughly equal to the area of the precursor cell from the first generation, which is equal to

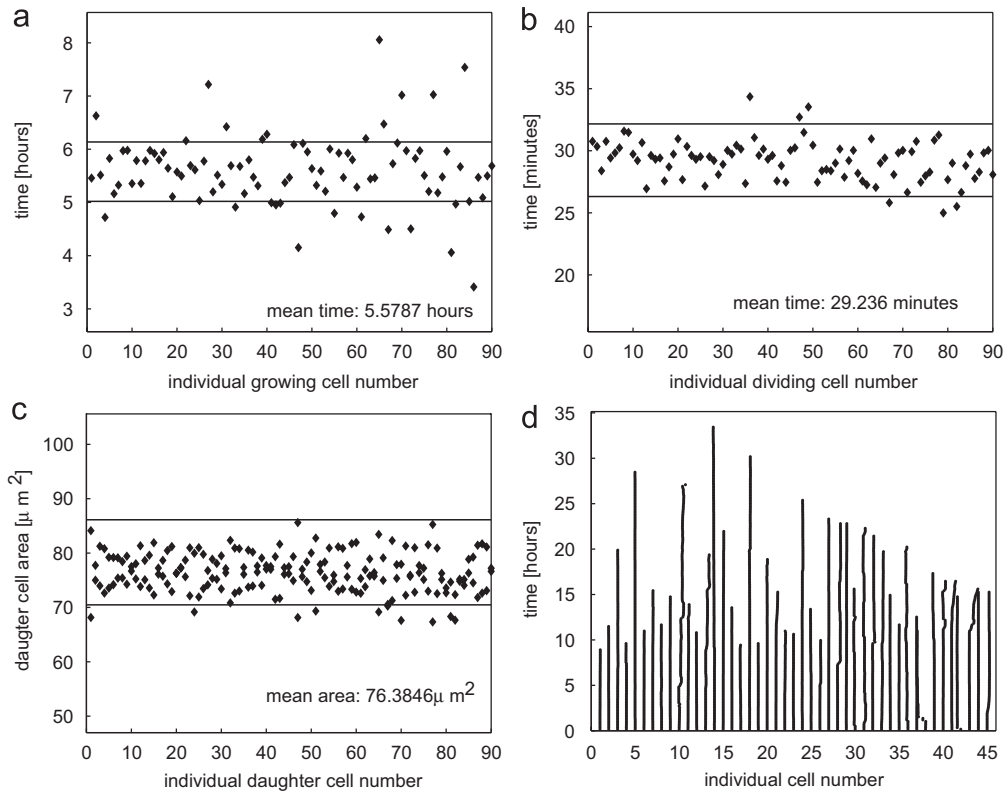


Fig. 8. (a) distribution of the time needed for doubling of the cell area; (b) distribution of the time needed to complete cell division; (c) distribution of the areas of daughter cells directly after their formation; solid lines in (a)–(c) show the 10% interval around the average values; (d) distribution of the areas of resting cells plotted from the time of their formation to the time of initiation of their growth; only cells resting for at least 8 h are presented. All data come from a simulation of the randomly growing clusters of tumour cells, Section 4.1.

78.5 μm^2 . The distribution of the areas of 90 daughter cells arising from consecutive divisions in a simulation of a randomly growing cluster of tumour cells described in Section 4.1 is shown in Fig. 8c. Almost all of them fall into the 10% interval around the ideal cell area. The uneven divisions arise mostly at the later stages of tumour development due to the more complex structure of the whole tumour cluster. The average area of all daughter cells is 76.38 μm^2 , that confirms our expectations that the cell areas do not significantly increase or decrease from one generation to another.

5.3. Areas of resting cells

The resting tumour cells do not show any mitotic activity but they are still part of the whole tissue and are exposed to the actions of other cells. In particular, they are subject to pressure enhanced by their growing neighbours, which can result in cell translocation, in deformations of the cell shape and in reducing the cell ability of maintaining their living properties. The behaviour of all cells in our model is fully dynamic and depends only on interactions with the neighbouring cells as well as on the environmental cues. In Fig. 8d we show how the area of the resting cells is preserved during the tumour development discussed in Section 4.1. For illustrative purposes, we show only these cells for which the resting time is longer than 8 h before they start proliferating. Most cells in our simulation have shorter resting times and, therefore, only 45 cells have been shown. Areas of all considered cells are plotted from the time of their formation to the time of initiation of their growth. All plots are almost vertical, that confirms small fluctuations in areas of the resting cells.

5.4. Single cell contribution to the growth of a whole cluster

Since our model takes explicitly into account not only the number of cells in the cluster, but also cell-to-cell interactions that lead to deformations of cell shapes and that can influence changes in cell areas, we present evidence that each growing cell contributes to the growth of the whole tumour by simultaneously increasing the total number of cells in the cluster and enlarging its area. This allows for a comparison with other models, such as continuous models or cellular automata models which deal with each of those aspects separately.

The number of cells in the tumour cluster changes from one to over 700 cells during the presented time of tumour growth, solid line in Fig. 9a. Because cells need time to grow, divide and become ready for a new cell cycle, and because every new proliferation can arise in certain time intervals, the changes in cell counts have a step-like form with variable lengths of separate plateaus. This is shown for an initial time period in Fig. 9b (solid line). During the initial 40 h of tumour development, the time intervals of constant cell counts are quite long, because the cluster contains a small number of cells and all of them are actively proliferating, during the later tumour development new cells are created more often and the plateaus exist infrequently and for a short period of time (less than an hour). However, the overall increase in cell count is slow, because most cells in large tumour clusters do not show any mitotic activity.

The total area of the tumour is computed as the sum of the areas of all individual cells. Its evolution during the whole time of tumour development is shown in Fig. 9a (dashed line), and magnifications of an initial time period

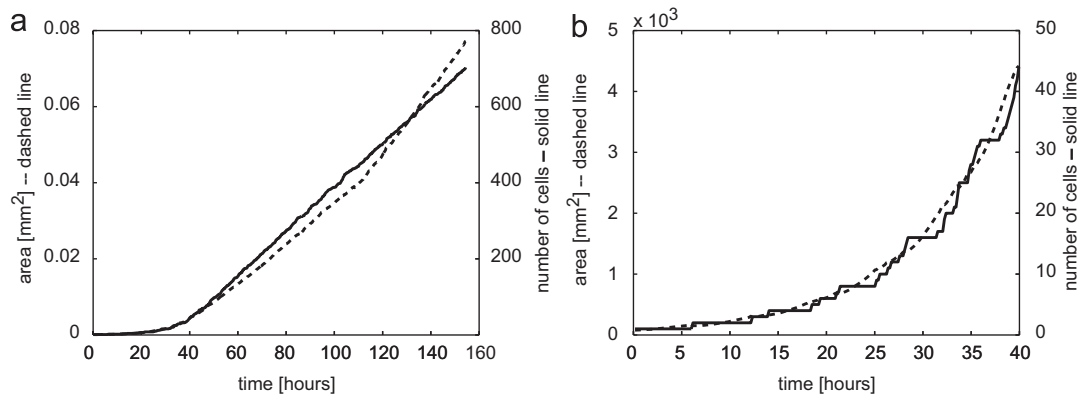


Fig. 9. (a) evolution of the total number of cells (solid line) and the total area of a tumour cluster (dashed line) in the whole time interval of 0–153 h; (b) magnification of the initial time interval of 0–40 h.

Table 1
Parameters of tumour growth: the cell count and the total tumour area

Time (hours)	0	20	40	60	80	100	120	140
Cell count	1	6	47	160	277	393	508	627
Tumour area (mm ²)	0.000078	0.00062	0.0046	0.014	0.024	0.035	0.048	0.066

0–40 h is presented in Fig. 9b (dashed line). Initially, the tumour area increases rapidly, because in small clusters all cells proliferate actively and expand freely in the surrounding medium. In the initial period of 20 h, the increase of tumour size is eight fold. At the later stages, the increase in total tumour area is slower due to the lower mitotic activity of cells in large clusters and to the more compact shape of the whole tumour tissue. Note, however, that by contrast with the cell count, even the initial evolution of the total tumour area has a continuous character.

The values of both parameters: the cell count and the total tumour area at the chosen time points are presented in Table 1.

6. Conclusions and future directions

We have presented a two-dimensional computational model of the growth and division of a single deformable eukaryotic cell. Our model is based on the immersed boundary method with distributed sources, and couples the continuous description of a viscous incompressible cytoplasm with the dynamics of elastic cells. Each cell in our model contains its own elastic plasma membrane, the point nucleus and individually regulated cell processes, such as cell growth and division, cell necrosis, cell-to-cell adhesion and the ability of sensing microenvironmental signals. This allows for a realistic representation of a single eukaryotic cell at rest and during its deformations, as well as for a representation of the whole tissue composed of such individual cells inhomogeneous in their shape, function and behaviour, but acting together as one complex organism. This approach enables one to focus on the biomechanical properties of individual cells and on communication between cells and their local microenvironment, whereas the global changes in the whole tissue can be observed simultaneously. The model can be used to investigate to what extent certain features in the developing organisms are a result of changes in individual cells, or a consequence of cell collective behaviour.

The main advantage of the method presented here over other existing cell-based models is explicitly modelled cell membrane that allows to define all cell interactions on the level of cell membrane receptors. Moreover, due to its elasticity the whole cell can easily deform and acquire different shapes. The main features that distinguish our model from other single-cell-based models of tumour growth include the following: (1) our cell model is defined off-lattice in contrast to the cellular automata (Anderson, 2005; Dormann and Deutsch, 2002; Kansal et al., 2000) and cellular Potts (Scott et al., 1999; Jiang et al., 2005) models; (2) cells are fully deformable in contrast to centre-based models (Drasdo and Höhme, 2005) and cellular automata models; (3) cell deformations during its growth and division are continuous in contrast to lattice-based cellular Potts models and limited deformability in cell-centred models; (4) all cell-to-cell interactions are modelled locally along the cell boundaries in contrast to centre-based

interactions in Drasdo and Höhme (2005) and energy minimalisation of the cellular system in cellular Potts models (Scott et al., 1999; Jiang et al., 2005); (5) nutrients consumption is defined along the cell membranes that allow cells to sense different concentrations of external factors from different directions in contrast to the average concentration of external factors sensed by cells in cellular automata and cell-centred models; (6) all mechanical interaction use direct boundary forces that is unique among all models cited above.

Four different applications simulating the formation and growth of solid tumours in various geometrical configurations and with distinct conditions of their initiation and progression have been also discussed. We presented a simulation of the development of a two-dimensional cross section of a multicellular spheroid with random selection of proliferating cells due to the nutrient-rich medium surrounding the growing cluster. This simulation shows how individually growing cells self-organise into a compact roundish cell cluster. The nutrient-driven emergence of three phenotypically different subpopulations of tumour cells within one cluster has been shown, and their competition for the nutrient that leads to formation of finger-like cohorts of viable cells invading the external medium has been examined. Finally, the formation of tumours growing along the linear or circular cross sections of epithelial ducts has been also discussed and the development of two particular patterns of intraductal carcinomas—micropapillary and solid—have been presented. These four examples show a strength of our computational approach to include in our model various scenarios of tumour growth, different conditions of its development and different geometrical configurations of tumour clusters and surrounding normal tissues.

We have restricted ourselves to present in this paper only applications relevant to modelling the formation and growth of early tumours, but the model can be employed in modelling other phases of tumour progression. In particular, it is easy to trace clones of cells that emerged from a common predecessor. Fig. 10a shows two coexisting cell clones that arose from two different cells during the development of the presented cell cluster. In this example both clones have exactly the same properties, so we just can inspect the spacial structure and mixing of both populations. It is in fact interesting that the white clone became separated into two disjoint regions by the grey clone. In further research it is possible to consider that one of the cell clones carries some specific gene mutations that give it a certain proliferative advantage over the second clone, and we can investigate patterns and fitness of clonal expansion, the emergence of new genotypically and phenotypically distinct cells that can lead to cell detachment and colonisation of the surrounding tissue.

Our model can be also used to model the growth of many other multicellular tissues and organisms. An earlier version of this model has been applied to investigate the formation of normal and abnormal folding in the human

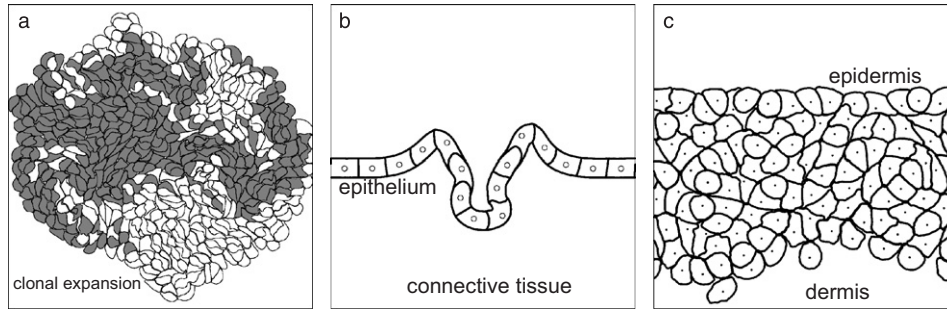


Fig. 10. Future possible areas of application of the presented model: (a) clonal mutant expansion within a cluster of growing cells; (b) renewal and diseases of epithelial crypts; (c) turnover of skin cells and wound healing.

placental trophoblast (Rejniak et al., 2004). The similar kind of geometry is also characteristic for epithelial crypts of intestines (compare Fig. 10b for a very simple representation of the crypt) and our model can be adjusted to investigate cell renewal, differentiation and migration along the crypts as well as certain diseases of cryptal epithelium. The outward tissue folding in the placental trophoblast (evagination) that has been already modelled in Rejniak et al. (2004) is considered to be an initial form of the outgrowth of a placental villous tree, so an appropriate modification of our model can be used to simulate branching morphogenesis in lungs or blood veins. Another possible application may involve a model of stratified epithelium in the skin as sketched in Fig. 10c. This may involve introducing different types of cell, with different geometry, physicochemical properties and functions, as well as distinct cell processes, such as cell apoptotic death or epidermal differentiation. The cell turnover and renewal by stem cells as well as wound healing may be a subject of further applications of our model. Moreover, many problems in embryonic development are also a subject of our interest, including asymmetric cell divisions in developing *C. elegans*; emerging cell patterns in early nematode embryo; cell sorting in growing *Drosophila*; or cleavage formation in *Xenopus*.

We have discussed in this paper some simplifications of the current model that may be overcome in further versions by incorporating additional intra- and extracellular elements. It is also desirable to introduce a three-dimensional version of growing cells. Of course, both such extensions will increase the overall computational cost of numerical simulations. Another aspect that should be addressed in future versions of this model is development of parallel algorithms that can handle complexity of the model. This is a very challenging issue, since our model represents a class of numerical problems where the number of boundary points, their locations and common interactions are changing dynamically during the computation.

Acknowledgements

I would like to thank Professor Mark Chaplain for stimulating discussions and suggesting new biological

applications of the model presented here, and Professor Avner Friedman for his invaluable comments to the first version of this manuscript. I also thank Dr Wiktor Gonet for his help in preparing the final version of this paper. The work presented here has been partially supported by the Mathematical Biosciences Institute at the Ohio State University under agreement No. 0112050 with the U.S. National Science Foundation.

Appendix A. Numerical implementation

We implement our model using finite difference schemes and the fast Fourier transform method for solving the Navier–Stokes equations. Interactions between the regular fluid grid and the material points on cell boundaries, on the boundaries of the basement membranes and at the cell nuclei are implemented using the discrete approximation to the Dirac delta function. The numerical scheme is described in Section A.1. The numerical algorithm for solving the whole coupled system is presented in Section A.2. A choice of computational and physical parameters is discussed in Section A.3.

A.1. Discretisation

In order to numerically implement the model described above, we discretise a square fluid domain $\Omega = [-L, L] \times [-L, L]$ using a uniform square grid of size $N \times N$ nodes with a mesh width $h = 2L/N$. We impose periodic boundary conditions on the fluid domain, because of the fast Fourier method used to solve the system. The Navier–Stokes equations (1) are discretised as follows:

$$\begin{aligned} \rho \left(\frac{u_r^{n+1} - u_r^n}{\Delta t} + \sum_{s=1}^2 u_s^n D_s^\pm u_r^n \right) \\ = -D_r^0 p^{n+1} + \mu \sum_{s=1}^2 D_s^+ D_s^- u_r^{n+1} + \frac{\mu}{3\rho} D_r^0 s^n + f_r^n, \end{aligned}$$

$$\rho \sum_{s=1}^2 D_s^0 u_s^{n+1} = s^n, \quad (16)$$

where $r = 1, 2$ denotes the first and second vector field components, and D^+ , D^- , D^0 and D^\pm are the forward, backward, central and upwind spatial difference operators, respectively.

Similarly, the cell plasma membranes are represented by Lagrangian points \mathbf{X}_l with boundary points separation of $\Delta l \approx h/2$. The computation proceeds in time steps of duration Δt . Eqs. (2)–(4) are then discretised as follows:

$$\begin{aligned}
 s^n(\mathbf{x}) &= \sum_{k \in \mathbb{Z}^+} S_+^n(\mathbf{Y}_k, t) \delta_h(\mathbf{x} - \mathbf{Y}_k) \\
 &\quad + \sum_{m \in \mathbb{Z}^-} S_-^n(\mathbf{W}_m, t) \delta_h(\mathbf{x} - \mathbf{W}_m), \\
 \mathbf{f}^n(\mathbf{x}) &= \sum_l \mathbf{F}^n(\mathbf{X}_l) \delta_h(\mathbf{x} - \mathbf{X}_l) \Delta l, \\
 \mathbf{u}^{n+1}(\mathbf{X}) &= \sum_{i,j} \mathbf{u}^{n+1}(\mathbf{x}_{i,j}) \delta_h(\mathbf{x}_{i,j} - \mathbf{X}) h^2, \\
 \mathbf{X}^{n+1} &= \mathbf{X}^n + \Delta t \cdot \mathbf{u}^{n+1}(\mathbf{X}). \tag{17}
 \end{aligned}$$

If the basement membranes are present, they are represented by Lagrangian points \mathbf{Z}_l with the same boundary points separation of $\Delta l \approx h/2$, and their governing equations are discretised analogously.

Interactions between the fluid and the immersed bodies are implemented using the discrete approximation $\delta_h(\mathbf{x})$ to the Dirac delta function. In our computations we use a symmetric continuous function of bounded support which is a product of two one-dimensional functions δ_h (Peskin, 1977), that is $\delta_h(\mathbf{x}) = \delta_h(x_1) \cdot \delta_h(x_2)$, where

$$\delta_h(r) = \begin{cases} \frac{1}{4h} \left(1 + \cos\left(\frac{\pi r}{2h}\right) \right) & \text{if } |r| < 2h, \\ 0 & \text{if } |r| \geq 2h. \end{cases} \tag{18}$$

The reaction-diffusion equations (14) for the evolution of the concentration of external factor γ are solved on the regular two-dimensional grid that coincides with the fluid grid. Here, Γ^n denotes a current (at time $n\Delta t$) configuration of all cells forming the tumour tissue, and D^+ , D^- are as before the forward and backward spatial difference operators, respectively.

$$\begin{aligned}
 \gamma^{n+1}(\mathbf{x}) &= \gamma^n(\mathbf{x}) + \Delta t \mathcal{D}_\gamma \sum_{s=1}^2 D_s^+ D_s^- \gamma^n(\mathbf{x}) \\
 &\quad - \underbrace{\Delta t \mathcal{V}_\gamma \frac{\gamma^n(\mathbf{x})}{\kappa_\gamma + \gamma^n(\mathbf{x})}}_{\text{if } \mathbf{x} \in \Theta_{\Gamma^n}}. \tag{19}
 \end{aligned}$$

A.2. Algorithm

The numerical algorithm for the full coupled system (in its most general form including the presence of the basement membranes and chemical gradients) can be outlined as follows. At the end of a time step n we are given values of the fluid velocity field \mathbf{u}^n , concentration of the external factor γ^n , the configuration of the immersed

boundary points \mathbf{X}^n on the cell plasma membranes, positions of cell nuclei \mathbf{Y}^n and the configuration of the material points \mathbf{Z}^n on the basement membranes. These values are updated at the next time step in the following way:

1. Inspect the concentration of oxygen γ^n in the micro-environments of all quiescent cells to determine which cells become necrotic; inspect all quiescent cells to determine which of them is exposed to the highest level of oxygen and will start growing; update the levels of oxygen concentration γ^{n+1} by computing rates of its consumption in the vicinity of tumour cells.
2. Determine the source distribution S_+^n at the nuclei of growing cells and the balancing sink distribution S_-^n in the fluid domain outside the cells, then spread these values to the neighbouring grid points to determine the local growth rate s^n of the fluid.
3. Calculate the total force density \mathbf{F}^n at the cell boundaries, including the membrane adjacent forces, cell-to-cell adhesion–repulsion forces, cell-to-basement membrane forces and contractile forces in the dividing cells. Spread these values to the neighbouring grid points to determine the forces \mathbf{f}^n on the fluid.
4. Solve the Navier–Stokes equations for the fluid velocity field \mathbf{u}^{n+1} by using the fast Fourier algorithm.
5. Interpolate the fluid velocity field \mathbf{u}^{n+1} to each immersed boundary point on cell membranes, on the basement membranes and to each cell nuclei. Compute new positions of \mathbf{X}^{n+1} , \mathbf{Y}^{n+1} and \mathbf{Z}^{n+1} by moving them at the local fluid velocity using a forward Euler step.

Three snapshots showing the methodology of the immersed boundary method are shown in Fig. 11. The boundary forces and point sources (Fig. 11a) are spread to the fluid grid to solve the Navier–Stokes equations for the fluid flow (Fig. 11b) that is then interpolated to the material points to find the boundary velocities (Fig.11c). All snapshots are taken from the same iteration step of a simulation of a growing intraductal micropapillary pattern discussed in Section 4.3.

A.3. Choice of computational parameters

Since we model the cell cytoplasm as a homogeneous continuum, the lack of its internal cytoskeleton is compensated by choosing values of the fluid viscosity and fluid density that correspond to the network part of the cytoplasm. It is reported in Laurent et al. (2003) that viscosity of the elastic cortical cytoskeletal network associated with actins and the plasma membrane in the adherent epithelial cells is in the range of 50–140 g/(cm s). Because most tumours arise from epithelial tissues, we take the fluid viscosity $\mu = 100$ g/(cm s) for all numerical computations. It is also reported in Dembo and Harlow (1986) that the network part of cytoplasm has a density $\rho = 1.35$ g/cm³ and this value is taken in our numerical

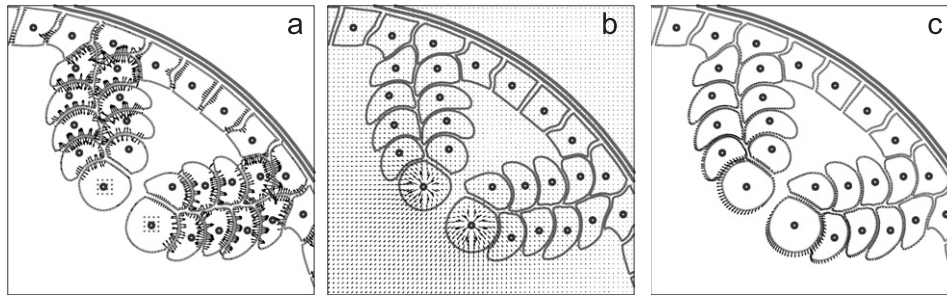


Fig. 11. Three snapshots taken from the same iteration step of a simulation of a growing intraductal micropapillary carcinoma discussed in Section 4.3 are used here to illustrate methodology of the immersed boundary method: (a) two point sources defined at the nuclei of two top cells are spread to the 16 points in the fluid grid (grey dots around the cell nuclei); boundary forces arising from adhesion–repulsion between separate cells (here mostly repulsion) and from deformation of cell boundaries (however, here the repulsive forces dominate); (b) the radially symmetric flows produced by two point sources are influenced by the cell-to-cell repulsive forces and the final fluid flow is directed mostly toward the free boundaries of the growing cells; (c) the cell boundary points move at the local fluid velocity, thus the cell expansion follows the fluid flow.

implementation. The strength of fluid sources in our model is identical in all growing cells and has been determined computationally to match the dynamics of a proliferating cell (Alberts et al., 2002, pp. 1034–1035). A good comparison has been achieved for the source strength $\mathcal{S}_0 = 2 \times 10^{-7}$ g/s. The value of each sink strength is chosen in a way to balance all fluid sources and thus it depends on the number of actually growing cells. The elastic properties of tumour cells have been achieved by an appropriate choice of the spring stiffness constants. It has been estimated in Laurent et al. (2003) that the rigidity of the elastic cortical cytoskeletal network associated with the plasma membrane in the adherent epithelial cells is in the range 490–850 g/(cm s²). In our numerical computations, we take $\mathcal{F}_{adj} = 500$ g/(cm s²) as a stiffness constant of all adjacent springs. The forces needed to separate two cells are estimated to be about 10³ g cm/s² per cm² of cell area (Bell, 1978). However, tumour cells are known to have weaker adhesive connections than normal cells, and thus a smaller force may be sufficient to break the cell-to-cell adhesive connections in tumours. In all numerical computations we use $\mathcal{F}_{adh} = 100$ g/(cm s²) for stiffness of the adhesive forces. In normal living cells the time needed to complete the process of cytokinesis is much shorter than the whole process of mitosis and cell growth. It is shown in (Alberts et al., 2002, pp. 1034–1035) for an epithelial cell in the lung, that cytokinesis lasts no more than 50 min, whereas the whole process of mitosis takes more than 6 h. Therefore, the value of the contractile spring stiffness $\mathcal{F}_{div} = 5 \times 10^7$ g/(cm s²) has been determined computationally in such a way, that the time needed to complete the process of cell division is no longer than 10% of the overall time of cell growth. For the model of nutrient-dependent tumour growth we take the rates of oxygen concentration and consumption that have been reported in a series of experimental papers on the in vitro growth of multicellular spheroids (Casciari et al., 1992; Freyer and Sutherland, 1985, 1986a, b), the optimal oxygen concentration $\gamma_0 = 0.28$ mM, maximal oxygen consumption rate $\mathcal{V}_\gamma = 2.36 \times 10^{-7}$ g/(cm³ s), Michaelis constant $\kappa_\gamma =$

0.046 mM, necrotic oxygen level $\gamma_{min} = 0.0082$ mM. The value of oxygen diffusion $\mathcal{D}_\gamma = 10^{-6}$ cm²/s in the living tissues has been reported in Swabb et al. (1974).

The average diameter of an individual cell is 10 μ m. The computational domain corresponds to the tissue of size 700 μ m \times 700 μ m, and the size of the fluid grid, $N = 512$, was chosen such that the support of a discrete Dirac delta function for the fluid source is entirely embedded in the body of a growing cell. The time step Δt must satisfy the CLF stability condition: $\Delta t \leq h/\|\mathbf{u}^n\|$. Resting lengths of all springs are equal to the half of mesh width, whereas radii of all microenvironments are equal to the mesh width. Typically, a cluster of first 50 cells is generated in a few hours on a one-processor (2.7 GHz) personal computer. However, the computational time increases with the number of cells involved, due to an increased number of dynamical re-arrangements of cell-to-cell adhesion links.

References

- Alarcón, T., Byrne, H.M., Maini, P.K., 2003. A cellular automaton model for tumour growth in inhomogeneous environment. *J. Theoret. Biol.* 225, 257–274.
- Alberts, B., Bray, D., Lewis, J., Raff, M., Roberts, K., Watson, J.D., 2002. *Molecular Biology of the Cell*, fourth ed. Garland, New York.
- Anderson, A.R.A., 2005. A hybrid mathematical model of solid tumour invasion: the importance of cell adhesion. *Math. Med. Biol.* 22, 163–186.
- Anderson, A.R.A., Chaplain, M.A.J., 1998. Continuous and discrete mathematical models of tumour-induced angiogenesis. *Bull. Math. Biol.* 60, 857–899.
- Anderson, A.R.A., Chaplain, M.A.J., Newman, E.L., Steele, R.J.C., Thompson, A.M., 2000. Mathematical modelling of tumour invasion and metastasis. *J. Theoret. Med.* 2, 129–154.
- Araujo, R.P., McElwain, D.L.S., 2004. A history of the study of solid tumour growth: the contribution of mathematical modelling. *Bull. Math. Biol.* 66, 1039–1091.
- Batchelor, G.K., 2000. *An Introduction to Fluid Dynamics*. Cambridge Mathematical Library Edition, Cambridge University Press, Cambridge.
- Bell, G.I., 1978. Models for specific adhesion of cells to cells. *Science* 200, 618–627.
- Bertuzzi, A., Gandolfi, A., 2000. Cell kinetics in a tumor cord. *J. Theoret. Biol.* 204, 587–599.

- Bottino, D.C., 1998. Modeling viscoelastic networks and cell deformation in the context of the immersed boundary method. *J. Comp. Phys.* 147, 86–113.
- Bottino, D.C., Fauci, L.J., 1998. A computational model of amoeboid deformation and locomotion. *Eur. Biophys. J.* 27, 532–539.
- Breward, C.J.W., Byrne, H.M., Lewis, C.E., 2002. The role of cell-cell interactions in a two-phase model for avascular tumour growth. *J. Math. Biol.* 45, 125–152.
- Byrne, H.M., Preziosi, L., 2003. Modelling solid tumour growth using the theory of mixtures. *Math. Med. Biol.* 20, 341–366.
- Byrne, H.M., King, J.R., McElwain, D.L.S., Preziosi, L., 2003. A two-phase model of solid tumour growth. *Appl. Math. Lett.* 16, 567–573.
- Casciari, J.J., Sotirchos, S.V., Sutherland, R.M., 1992. Variations in tumor cell growth rates and metabolism with oxygen concentration, glucose concentration, and extracellular pH. *J. Cell Physiol.* 151, 386–394.
- Chaplain, M.A.J., Graziano, L., Preziosi, L., 2006. Mathematical modelling of the loss of tissue compression responsiveness and its role in solid tumour development. *Math. Med. Biol.* 23, 197–229.
- Conlon, I., Raff, M., 2003. Differences in the way a mammalian cell and yeast cells coordinate cell growth and cell-cycle progression. *J. Biol.* 2, 1–10.
- Conlon, I.J., Dunn, G.A., Mudge, A.W., Raff, M.C., 2001. Extracellular control of cell size. *Nat. Cell Biol.* 3, 918–921.
- Cristini, V., Bławdziewicz, J., Loewenberg, M., 2001. An adaptive mesh algorithm for evolving surfaces: simulations of drop breakup and coalescence. *J. Comput. Phys.* 168, 445–463.
- Cytrynbaum, E.N., Scholey, J.M., Mogilner, A., 2003a. A force balance model of early spindle pole separation in *Drosophila* embryos. *Biophys. J.* 84, 757–769.
- Cytrynbaum, E.N., Rodionov, V., Mogilner, A., 2003b. Computational model of dynein-dependent self-organization of microtubule asters. *J. Cell Sci.* 117, 1381–1397.
- Dembo, M., Harlow, F., 1986. Cell motion, contractile networks, and the physics of interpenetrating reactive flow. *Biophys. J.* 50, 109–121.
- Dillon, R.H., Fauci, L.J., 2006. Biofluidmechanics of reproduction. *Annu. Rev. Fluid Mech.* 38, 371–394.
- Dillon, R., Othmer, H.G., 1999. A mathematical model for outgrowth and spatial patterning of the vertebrate limb bud. *J. Theoret. Biol.* 197, 295–330.
- Dillon, R.H., Fauci, L.J., Omoto, Ch., 2003. Mathematical modeling of axoneme mechanics and fluid dynamics in ciliary and sperm motility. *Dyn. Continuous Discrete Impulsive Syst. Ser. A* 10, 745–757.
- Dormann, S., Deutsch, A., 2002. Modeling of self-organized avascular tumor growth with a hybrid cellular automaton. *In Silico Biol.* 2, 393–406.
- Drasdo, D., Höhme, S., 2003. Individual-based approaches to birth and death in avascular tumors. *Math. Comput. Modelling* 37, 1163–1175.
- Drasdo, D., Höhme, S., 2005. A single-cell-based model of tumour growth in vitro: monolayer and spheroids. *Phys. Biol.* 2, 133–147.
- Fall, Ch.P., Marland, E.S., Wagner, J.M., Tyson, J.J., 2002. *Computational Cell Biology*. Springer, Berlin.
- Folkman, J., Hochberg, M., 1973. Self-regulation of growth in three dimensions. *J. Exp. Med.* 138, 745–753.
- Franks, S.J., Byrne, H.M., Underwood, J.C.E., Lewis, C.E., 2005. Biological inferences from a mathematical model of comedo ductal carcinoma in situ of the breast. *J. Theoret. Biol.* 232, 523–543.
- Friedman, A., 2004. A hierarchy of cancer models and their mathematical challenges. *Discrete Continuous Dynamical Syst. Ser. B* 4, 147–159.
- Freyer, J.P., Sutherland, R.M., 1985. A reduction in the in situ rates of oxygen and glucose consumption of cells on EMT6/Ro spheroids during growth. *J. Cell Physiol.* 124, 516–524.
- Freyer, J.P., Sutherland, R.M., 1986a. Regulation of growth saturation and development of necrosis in EMT6/Ro multicellular spheroids by the glucose and oxygen supply. *Cancer Res.* 46, 3513–3520.
- Freyer, J.P., Sutherland, R.M., 1986b. Proliferative and clonogenic heterogeneity of cells from EMT6/Ro multicellular spheroids induced by the glucose and oxygen supply. *Cancer Res.* 46, 3504–3512.
- Galle, J., Loeffler, M., Drasdo, D., 2005. Modeling the effect of deregulated proliferation and apoptosis on the growth dynamics of epithelial cell populations in vitro. *Biophys. J.* 88, 62–65.
- Givelberg, E., Bunn, J., 2003. A comprehensive three-dimensional model of the cochlea. *J. Comput. Phys.* 191, 377–391.
- He, X., Dembo, M., 1997. On the mechanics of the first cleavage division of the sea urchin egg. *Exp. Cell Res.* 233, 252–273.
- Hoppensteadt, F.C., Peskin, Ch.S., 1992. *Mathematics in Medicine and The Life Sciences*. Springer, Berlin.
- Jiang, Y., Pjesivac-Grbovic, J., Cantrell, Ch., Freyer, J.P., 2005. A multiscale model for avascular tumour growth. *Biophys. J.* 89, 3884–3894.
- Kansal, A.R., Torquato, S., Chiocca, E.A., Deisboeck, T.S., 2000. Emergence of a subpopulation in a computational model of tumour growth. *J. Theoret. Biol.* 207, 431–441.
- Keener, J., Sneyd, J., 1998. *Mathematical Physiology*. Springer, Berlin.
- Khismatullin, D.B., Renardy, Y., Cristini, V., 2003. Inertia-induced breakup of highly viscous drops subjected to simple shear. *Phys. Fluids* 15, 1351–1354.
- Laurent, V.M., Planus, E., Fodil, R., Isabey, D., 2003. Mechanical assessment by magnocytometry of the cytosolic and cortical cytoskeletal compartments in adherent epithelial cells. *Biorheology* 40, 235–240.
- Lim, S., Peskin, C.S., 2004. Simulations of the whirling instability by the immersed boundary method. *SIAM J. Sci. Comput.* 25, 2066–2083.
- Lodish, H., Berk, A., Matsudaira, P., Kaiser, Ch.A., Krieger, M., Scott, M.P., Zipursky, S.L., Darnell, J., Lodish, H.F., 2003. *Molecular Cell Biology*. Freeman, New York.
- Lubkin, S.R., Jackson, T., 2002. Multiphase mechanics of capsule formation in tumors. *J. Biomech. Eng.* 124, 237–243.
- Mansury, Y., Deisboeck, T.S., 2003. The impact of “search precision” in an agent-based tumor model. *J. Theoret. Biol.* 224, 325–337.
- Mansury, Y., Kimura, M., Lobo, J., Deisboeck, T.S., 2002. Emerging patterns in tumour systems: simulating the dynamics of multicellular clusters with an agent-based spatial agglomeration model. *J. Theoret. Biol.* 219, 343–370.
- Merks, R.M.H., Glazier, J.A., 2005. A cell-centered approach to developmental biology. *Physica A* 352, 113–130.
- Mueller-Klieser, W., 1978. Multicellular spheroids. *J. Cancer Res. Clin. Oncol.* 113, 101–122.
- Nowell, P.C., 1976. The clonal evolution of tumor cell populations. *Science* 194, 23–28.
- Patel, A.A., Gawlinski, E.E., Lemieux, S.K., Gatenby, R.A., 2001. A cellular automaton model of early tumor growth and invasion: the effects of native tissue vascularity and increased anaerobic tumor metabolism. *J. Theoret. Biol.* 213, 315–331.
- Peskin, C.S., 1972. Flow patterns around heart valves: a numerical method. *J. Comput. Phys.* 10, 252–271.
- Peskin, C.S., 1977. Numerical analysis of blood flow in the heart. *J. Comput. Phys.* 25, 220–252.
- Peskin, C.S., 2002. The immersed boundary method. *Acta Numer.* 11, 479–517.
- Pollard, T.D., Earnshaw, W.C., 2004. *Cell Biology*. Saunders Co Ltd.
- Pozrikidis, C., 2003. *Modeling and Simulation of Capsules and Biological Cells*. Chapman & Hall, London.
- Preziosi, L., 2003. *Cancer Modelling and Simulation*. CRC Press, Boca Raton.
- Rejniak, K.A., 2005. A single-cell approach in modeling the dynamics of tumor microregions. *Math. Biosci. Eng.* 2, 643–655.
- Rejniak, K.A., Dillon, R.H., 2007. A single-cell-based model of the ductal tumour microarchitecture. *Comput. Math. Methods Med.* 8(1), doi:10.1080/17486700701303143.
- Rejniak, K.A., Kliman, H.J., Fauci, L.J., 2004. A computational model of the mechanics of growth of the villous trophoblast bilayer. *Bull. Math. Biol.* 66, 199–232.

- Schwegler, H., Tarumi, K., Gerstmann, B., 1985. Physico-chemical model of protocell. *J. Math. Biol.* 22, 335–348.
- Scott, E.L., Britton, N.F., Glazier, J.A., Zajac, M., 1999. Stochastic simulation of benign avascular tumour growth using the Potts Model. *Math. Comput. Modelling* 30, 183–198.
- Sherratt, J.A., Chaplain, M.A.J., 2001. A new mathematical model for avascular tumour growth. *J. Math. Biol.* 43, 291–312.
- Sutherland, R.M., 1988. Cell and environment interactions in tumor microregions: the multicell spheroid model. *Science* 240, 177–184.
- Sutherland, R.M., McCredie, J.A., Inch, W.R., 1971. Growth of multicell spheroids in tissue culture as a model of nodular carcinomas. *J. Natl Cancer Inst.* 46, 113–120.
- Swabb, E.A., Wei, J., Gullino, P.M., 1974. Diffusion and convection in normal and neoplastic tissue. *Cancer Res.* 34, 2814–2822.
- Turner, A., Sherratt, J.A., 2002. Intracellular adhesion and cancer invasion: a discrete simulation using the extended Potts model. *J. Theoret. Biol.* 216, 85–100.
- Watton, P.N., Luo, X.Y., Wang, X., Bernacca, G.M., Molloy, P., Wheatley, D.J., 2007. Dynamic modelling of prosthetic chorded mitral valves using the immersed boundary method. *J. Biomech.* 40, 613–626.
- Wollman, R., Cytrynbaum, E.N., Jones, J.T., Meyer, T., Scholey, J.M., Mogilner, A., 2005. Efficient chromosome capture requires a bias in the “search-and-capture” process during mitotic-spindle assembly. *Curr. Biol.* 15, 828–832.
- Zhang, L., Athale, Ch.A., Deisboeck, T.S., 2006. Development of a three-dimensional multiscale agent-based tumor model: simulating gene-protein interaction profiles, cell phenotypes and multicellular patterns in brain cancer. *J. Theoret. Biol.* 244, 96–107.